Available online at www.sciencedirect.com
SCIENCE DIRECT®
Infrared Physics & Technology 47 (2005) 15–21
INFRARED PHYSICS & TECHNOLOGY
www.elsevier.com/locate/infrared

Multi-band and broad-band infrared detectors based on III–V materials for spectral imaging instruments

S.V. Bandara *, S.D. Gunapala, J.K. Liu, S.B. Rafol, C.J. Hill, D.Z. Ting, J.M. Mumolo, T.Q. Trinh

Jet Propulsion Laboratory, California Institute of Technology 4800, Oak Grove Drive, Pasadena, CA 91109, USA

Available online 13 April 2005

Abstract

Quantum well infrared photodetector technology has shown remarkable success by realizing large-format focal plane arrays in both broad-bands and in multi-bands. The spectral response of these detectors based on the III–V material system are tailorable within the mid and long wavelength IR bands (~3–25 μm) and possibly beyond. Multi-band and broad-band detector arrays have been developed by vertically integrating stacks of multi quantum wells tailored for response in different wavelengths bands. Each detector stack absorbs photons within the specified wavelength band while allowing the transmission other photons, thus efficiently permitting multiband detection. Flexibility in many design parameters of these detectors allows for tuning and tailoring the spectral shape according to application requirements, specifically for spectral imaging instruments.

PACS: 78.30.Fs; 78.67.De

Keywords: Quantum-well infrared photodetector; Multi-color; Tunable detectors; Thermal infrared

1. Introduction

Infrared spectroscopy is a widely used technique in both ground and space-based remote sensing instruments to obtain critical scientific information as well as real time detection and identification of targets. The mid to long-wavelength band (3–16 μm) of the infrared spectrum provides a wealth of information concerning surface temperatures and thermal properties of soils, rocks, vegetation, and man-made structures. Inferences based on thermal properties leads to the identification of surface materials and temperatures. In addition, infrared photons in the 3–16 μm wavelength band can excite rotational and

* Corresponding author. Tel.: +1 818 354 7377; fax: +1 818 393 4540.
E-mail address: sumith.v.bandara@jpl.nasa.gov (S.V. Bandara).

1350-4495/$ - see front matter
doi:10.1016/j.infrared.2005.02.006

vibrational modes of molecules, generating absorption or emission bands in the infrared spectrum. The shape and location of these bands uniquely identify the molecules that constitute the volume of a gas or atmosphere being investigated.

High resolution imaging spectrometers or interferometers performing such investigations require small-pixel, large-format focal plane arrays (FPAs) with high uniformity and operability. It would also be desirable to have low $1/f$ noise to reduce the calibration burden and increase the temporal stability, i.e. improve measurement accuracy and precision. The GaAs/AlGaAs-based Quantum Well Infrared Photodetector (QWIP) technology is an excellent choice for the development of such large format FPAs due to its mature fabrication and processing technology [1,2]. QWIP technology has shown remarkable success in advancing low-cost, highly uniform, high-operability, large-format FPAs [3–5]. In addition, multi-quantum well (MQW) parameters of the GaAs/$Al_xGa_{1-x}As$ based QWIPs can be varied over a range wide enough to enable light detection at any wavelength range from 6 to 25 μm [1,2]. By adding a few monolayers of $In_yGa_{1-y}As$ during the GaAs quantum well growth, the short wavelength limit can be extended to 3 μm [6]. The spectral bandwidth of these detectors can be tuned from narrow ($\Delta\lambda/\lambda \sim 10\%$) to wide ($\Delta\lambda/\lambda \sim 40\%$), according to application requirements [7].

In order to cover a wider spectral range, these instruments require FPAs sensitive in wider wavelength bands. Such FPAs are feasible via (a) a multi-band FPA that consists of several narrow band (or broad-band) monolithically integrated QWIP stacks, or (b) a broad-band QWIP FPA [4,8,9]. Fig. 1 shows 8–12 μm spectral coverage using four narrow-band QWIPs and a single broad-band QWIP. The preceding multi-band design is more suitable for hyperspectral spectrometers that require pixels compatible with many very narrow spectral channels across the FPA. Pixels with a narrow spectral response produce less photocurrent noise due to the instrument background than a pixel with a broad spectral response. For imaging interferometers, a single broad-band detector covering the entire spectral band is preferred because of the complexity created by the spectral overlap between multiple bands [4,10]. However, if the required wavelength coverage is wider than that of a broad-band QWIP spectrum, the only option available is to utilize a multi-broad-band FPA. Recently we have delivered both types of QWIP FPAs: (a) a 640×512 four-band QWIP FPA for hyperspectral imager [8,9,11] and (b) a 640×512 dual-broad-band QWIP FPA for a miniature interferometer [4,10]. This article focuses on design issues of multi-band QWIP layer structures and the tailorability and tunability of the broad-band QWIP's spectral responsivity.

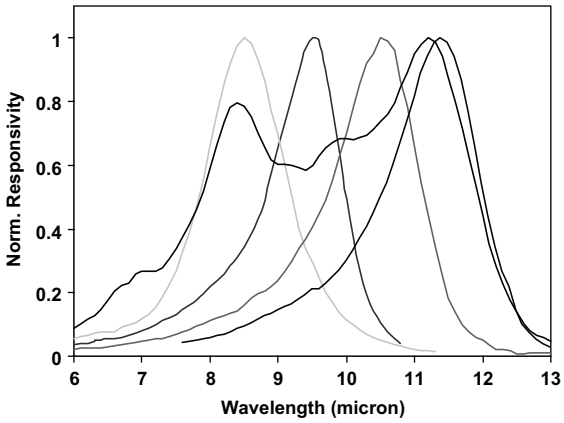

Fig. 1. Normalized specral responsivity of QWIPs covering 8–12 μm spectral band. The entire spectral band is covered by a single broad-band QWIP or by a four narrow band QWIPs.

2. Multi-band QWIPs

A 640×512 format spatially separated four-band QWIP (FPA) based on a InGaAs/GaAs/AlGaAs material system has been developed for a hyperspectral imaging instrument sensitive in selected wavelength bands within a wavelength range from 4 to 15.5 μm [8,9,11]. Fig. 2 shows the schematic layer diagram of the four-band detector array consisting of four QWIP stacks. The area array is divided into four sub areas each consisting 640×128 pixels, that are sensitive in the 4–5.5 μm, 8.5–10 μm, 10–12 μm, and 13–15.5 μm wavelength bands. The actual device structure consists of a 0.6 μm thick stack of 15-period MQW structure (D1), a 1.1 μm thick stack of 25-

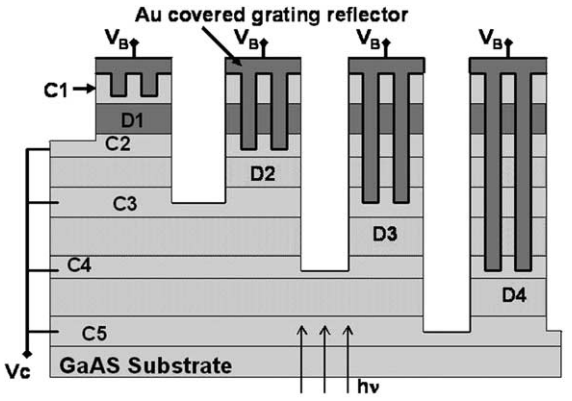

Fig. 2. A schematic of the layer diagram and pixel isolation scheme of four-band detector array. D1, D2, D3, & D4 represent MQW layers designed to respond at 4–5.5 μm, 8.5–10 μm, 10–12 μm, and 13–15.5 μm wavelength bands. C1 to C5 are heavily doped contact layers. The gold-coated reflective etched gratings are fabricated on each pixel allowing absorption of normally incident light. These gratings also serve as contacts to the active detector while shorting the unwanted top detectors. The unwanted bottom detectors are electrically shorted from the outside of the array.

period MQW structure (D2), a 1.2 μm thick stack of 25-period MQW structure (D3), and a 1.8 μm thick stack of 30-period MQW structure (D4). The quantum well parameters of D1, D2, D3, and D4 were designed to respond at 4–5.5 μm, 8.5–10 μm, 10–12 μm, and 13–15.5 μm wavelength ranges, respectively. The quantum well width and barrier Al-composition of the detectors are D1: 34 Å, 0.31%, D2: 50 Å, 0.23%, D3: 56 Å, 0.19, and D4: 75 Å, 0.15 respectively. The photosensitive MQW stacks were separated by heavily doped intermediate GaAs contact layers, with thickness ranging from 0.2 μm to 0.8 μm (see Fig. 2). The quantum wells in the D1, D2, D3 and D4 structures are doped with Si to a carrier density of $n = 2 \times 10^{18}\ \mathrm{cm}^{-3}$, $n = 6 \times 10^{17}\ \mathrm{cm}^{-3}$, $n = 4 \times 10^{17}\ \mathrm{cm}^{-3}$, and $n = 2 \times 10^{17}\ \mathrm{cm}^{-3}$ respectively.

As shown in Fig. 2, the FPA pixels are fabricated such that only a single color QWIP is active in each sub area during operation. Optimized two-dimensional (2-D) reflective gratings with deeper groove depths were utilized in this FPA in order to reflect light in preferred directions, allowing absorption within the active MQW layers of each IR band [8,12]. These gratings were created by dry etching and coated with Au. In addition to light coupling, these gratings serve as a contact to the active stack while shorting the unwanted top stacks. The unwanted bottom QWIP stacks were electrically shorted at the end of each detector pixel row and connected to a common ground. When the detector pixels are biased through the pixel top and the common ground, each pixel activates only a single QWIP stack and reads a photocurrent generated by photons absorbed within a single IR wavelength band.

Typically in QWIPs, the dark current is dominated by thermal excitation across the sub-band gap, which sets the operating temperature [1–6]. During the design, the longest wavelength QWIP device structure (D4) was optimized to minimize the dark current. This dark current is the highest among the four detectors because the smallest sub-band gap is associated with the longest-wavelength response. This was achieved by utilizing a bound-to-bound quantum well design with 600 Å thick barriers. Other QWIP device structures are designed to have a bound-to-continuum intersub-band absorption process, because the dark currents of these detectors are relatively small compared to the D4 detector [9]. Due to thickness restrictions set by the optical gratings, a lower number of periods and thinner barriers were used in the shorter wavelength detectors (D1, D2 and D3). In order to balance the lowered absorption quantum efficiency associated with fewer periods, the quantum wells are doped to a higher carrier density. Typically, this is not the preferred way to improve QWIP performance, because higher carrier density increases thermal excitation, i.e. dark current of the detector [1,2]. However, this is not a problem for the top three detectors, D1, D2, and D3 because they operate at a lower temperature determined by the longest wavelength detector, D4.

3. Broad-band QWIPs

The responsivity spectrum of a typical QWIP is inherently narrower and sharper, because the photoexcitation occurs between energy levels localized within the quantum wells that are separated by

thick barriers. Typically, the responsivity spectra of the *bound* and *quasibound* excited state QWIPs are much narrower ($\Delta\lambda/\lambda \sim 10\%$) than the *continuum* QWIPs ($\Delta\lambda/\lambda = 24\%$) [1,2]. This is due to the fact that, when the excited state is placed in the continuum band above the barrier, the energy width associated with the state becomes wide. The spectral band width of these QWIPs can be further increased by replacing single quantum wells with small superlattice structures, several quantum wells separated by thin barriers, in the multi-quantum well structure [7] (see Fig. 3). Such a scheme creates an excited state miniband due to overlap of the excited state wavefunctions of the quantum wells. Energy band calculations shows that excited state energy level spreading depends sharply on the with of the superlattice barrier at smaller thicknesses. Fig. 4 shows the experimentally measured spectral responsivity of the four different QWIP structures described in Table 1. These measurements were carried out under similar electric fields applied by adjusting the bias voltages across the detectors. The detector N1 is a typical narrow-band QWIP, while detectors B1, B2 and B3 are broad-band QWIPs with different superlattice barrier thicknesses (Ls) and number of periods (N_s). An identical quantum well used in all four

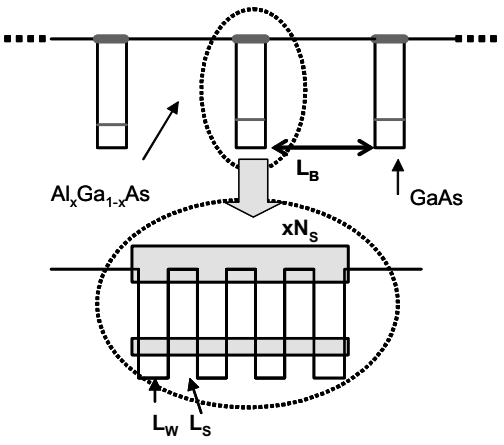

Fig. 3. Schematic band diagram of a typical narrow-band MQW (top) and a broad-band MQW (bottom). The broad-band MQW structure is created by replacing single quantum wells in the narrow-band structure by few period superlattices. The thin barriers (Ls) in the superlattice structure results in minibands due to coupling of wavefunctions.

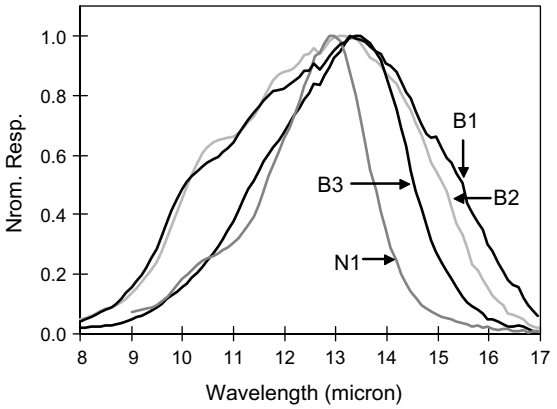

Fig. 4. Normalized spectral responsivity of a narrow band QWIP (N1) and three broad-band QWIPs (B1, B2, and B3). All four QWIPs have repeated nearly identical quantum well in different manners, as described in Table 2. Responsivity measurements were carried out under similar electric fields across the detectors.

QWIPs results in a same spectral peak wavelength except for a slight shift in N1 owing to the narrower width of the quantum well. Fig. 4 clearly shows a strong dependence of the spectral bandwidth ($\Delta\lambda/\lambda \sim 12$–$45\%$) on the superlattice barrier thickness of a broad-band QWIP.

Unlike in narrow band QWIPs, broad-band QWIPs show considerable spectral shape change with bias voltage, particularly near the cut-off wavelength region, as shown in Fig. 5. The cause of this long cut-off shift can be attributed to the finite energy spreading of the excited state in the superlattice structure used in broad-band QWIPs. The excited state energy levels associated with longer wavelengths are more strongly bound than those associated with shorter wavelengths. Therefore, it is required to apply a higher bias voltage to transport photoexcited electrons associated with longer wavelengths. The cause of this peak shift can be explained using the optical gain (g_p) which is defined by $R(\lambda) = (e/h)v\ \eta(\lambda)g_p(\lambda)$ where R is the responsivity, η is the absorption quantum efficiency (QE), e is the electronic charge, and hv is the photoexcitation energy [1,7]. For longer wavelengths, it is necessary to apply a higher bias voltage to obtain a reasonable non-zero value for g_p, while for shorter wavelengths g_p starts from zero bias. This can be attributed to the behavior of

Table 1
Design parameters of a narrow band QWIP (N1) and three broad-band QWIPs (B1, B2, and B3)

Detector	Well width (L_W) (Å)	QWIP barrier width (L_B) (Å)	Barrier Al% (x)	Superlattice barrier width (L_S) (Å)	# of wells in superlattice (N_S)
N1	65	600	16%	None	1
B1	70	600	15%	60	4
B2	70	600	15%	60	3
B3	70	600	15%	80	3

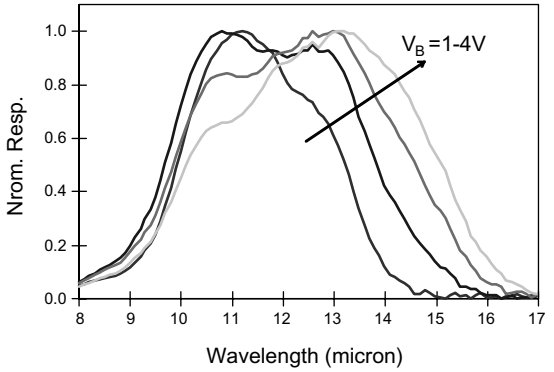

Fig. 5. Bias dependence spectral responsivity of a broad-band QWIP structure which is created by replacing single quantum wells in the narrow-band structure by few period superlattices.

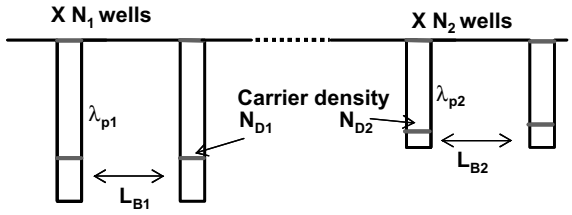

Fig. 6. Schematic band diagram of a "stack design" broad-band QWIP which consists of two stacks of MQW structures designed to respond at two different wavelengths within the required broad wavelength band.

transmission probability factor (γ) in g_p, i.e. $g_p \propto \gamma$. The γ is smaller for low energy photoexcited electrons, i.e. longer wavelength transitions, because those electrons need to tunnel through a barrier to contribute to the photocurrent (see the band diagram of a broad-band QWIP in Fig. 3).

4. Tuning and tailoring the broad-band QWIP spectra

This change in spectral shape due to the bias voltage is an undesirable property for spectral imaging instruments because it could complicate the calibration process. If the spectral shape is fixed, the operating bias voltage of the FPA can be used as a parameter to optimize instrument performance during the imaging of different targets against different backgrounds. In order to accommodate this flexibility, we have considered two alternate designs for broad-band QWIPs based on discrete narrow band QWIPs. Fig. 6 shows a schematic band diagram of the "stack design," which consists of two stacks of MQW structures designed to respond at two different wavelengths within the required broad wavelength band. A similar design scheme was used in the past for tunable multi-band QWIPs [13,14]. If the two MQW structures have dissimilar impedances, a disproportional bias voltage drop across the structures could lead to a dominant photocurrent response from a single structure. As the bias voltage changes, response could switch to the other structure, effectively acting as a voltage tunable detector [13,14]. Therefore, in order to keep the broad-band spectral shape unchanged, it is essential to design two MQW structures with similar impedances, at least within the desired operating temperatures and bias voltages.

Table 2 shows three different structural parameters for "stack design" broad-band QWIPs. Detector SB1 consists of two MQW structures, with similar barrier thickness and one designed for $\lambda p_1 = 6.8$ μm and the other for $\lambda p_2 = 8.5$ μm peak wavelength. Despite having a higher carrier density, the 6.8 μm QWIP has higher impedance than the 8.5 μm QWIP. Therefore, as the bias voltage increases, most of the bias drops across the

Table 2
Design parameters of three different "stack design" broad-band QWIPs

Design parameter	Detector SB1		Detector SB2		Detector SB3	
	Stack 1	Stack 2	Stack 1	Stack 2	Stack 1	Stack 2
Peak λ (μm)	6.8	8.5	11.2	14.0	11.4	13.4
# of wells	20	20	25	30	20	25
Well thickness (Å)	40(4%In)	48	56	75	59	70
Barrier thickness (Å)	300	300	400	500	400	500
Barrier Al%	28%	25%	19%	15%	18%	16%
Well doping (cm^{-3})	1.2×10^{18}	6×10^{17}	4×10^{17}	2×10^{17}	4×10^{17}	2×10^{17}

6.8 μm QWIP and then spreads over to the 8.5 μm QWIP. Fig. 7(a) shows the spectral peak wavelength switching from $\lambda p_1 = 6.8$ μm to $\lambda p_2 = 8.5$ μm within a small bias voltage change (from $V_B = 3.5$ to 5.0 V) demonstrating the highly sensitive wavelength tunability of the device. Unlike detector SB1, SB2 and SB3 were designed to produce minimal spectral shape changes as bias voltage is varied. Detector SB2 comprises two MQW structures with $\lambda p_1 = 11.2$ μm and $\lambda p_2 = 13.8$ μm while detector SB3 comprises two MQW structures with $\lambda p_1 = 11.4$ μm and $\lambda p_2 = 13.4$ μm peak wavelengths. In order to reduce the impedance of the shorter wavelength MQWs to the level of the longer wavelength MQWs, bound-to-continuum quantum wells with thinner barriers were utilized, with the design parameters shown in Table 2. The normalized spectral responsivity plots at different bias voltages in Fig. 7(b) shows nearly a unchanged broad-band spectrum of SB2 within a 1–2 V voltage range, while Fig. 7(c) demonstrates the nearly unchanged broad-band spectrum of SB3 within a 1–3 V voltage range.

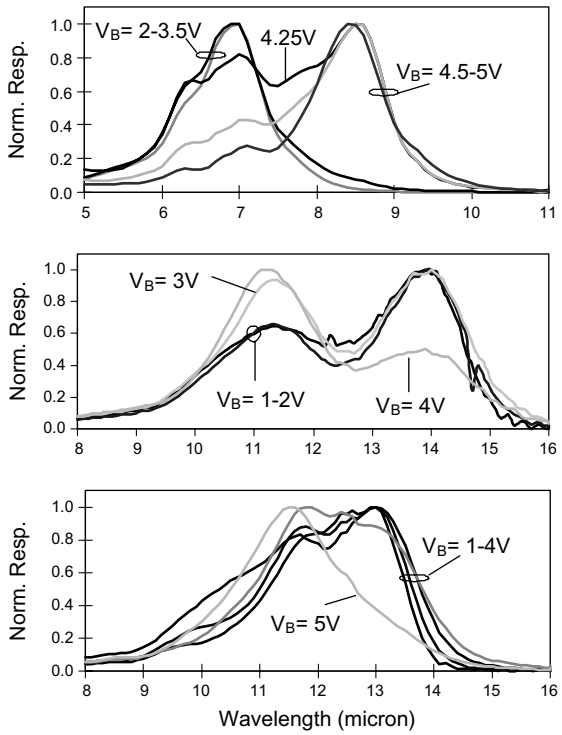

Fig. 7. Bias voltage dependence spectral responsivity of three different "stack design" QWIPs. (a) Due to unequal impedance of the two stacks, detector SB1 shows spectral tunability with the bias voltage. As shown in (b) & (c), SB2 and SB3 are designed to produce nearly unchanged spectra within the operating bias voltage range.

Fig. 8 shows a schematic band diagram of an "intermix design" broad-band QWIP consisting of multiple periods of alternatively placed dissimilar quantum wells designed to respond at $\lambda p_1 = 11.4$ μm and $\lambda p_2 = 13.4$ μm peak wavelengths. Each quantum well in the structure is separated by a 500 Å thick $Al_xGa_{1-x}As$ barrier with a bidirectionally-graded Al composition of $x = 18$–16%. The impedances of both types of quantum wells were kept at similar values by utilizing a bound-continuum design with higher doping density in shorter wavelength quantum wells. Fig. 9 shows the normalized spectral responsivity measured at different bias voltages. As designed, the broad-band spectral shape is nearly unchanged within a $V_B = 1$–4 V bias range. The higher responsivity at shorter wavelengths ($\lambda p_1 = 11.4$ μm) is attributed to the higher carrier density of the short wavelength quantum wells. One can obtain a smoother responsivity curve by properly

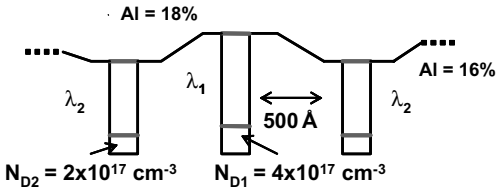

Fig. 8. Schematic band diagram of the "intermix design" of a broad-band QWIP consisting of multiple periods of alternatively placed, dissimilar quantum wells.

adjusting the doping densities of the quantum wells or by adding more longer-wavelength quantum wells to the MQW structure.

5. Summary

In summary, several methods for realizing broad-band QWIP FPAs for spectral imaging instruments have been discussed. The requisite spectral band can be covered by utilizing a single broad-band MQW or by stacking a few narrow band MQWs, thereby creating a multi-band detector. It is important to avoid a change in spectral shape due to the bias voltage of the broad-band FPAs utilized in spectral imaging instruments. Several alternatives to the typical broad-band QWIP design have been demonstrated. A "stack design" which consists of two MQW stacks produces a nearly fixed spectrum as well as a highly tunable spectrum according to the impedance of each stack.

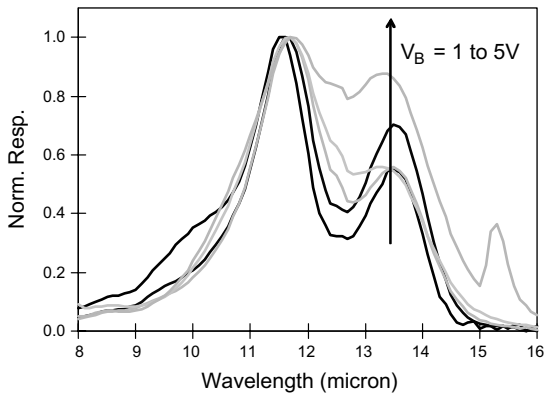

Fig. 9. Bias voltage dependence of the spectral responsivity of an "intermix design" broad-band QWIP.

Acknowledgments

The research described in this paper was carried out at the Jet Propulsion Laboratory, California Institute of Technology, and was partly sponsored by the National Aeronautics and Space Administration Offices of Aerospace Technology and Earth Sciences.

References

[1] B.F. Levine, J. Appl. Phys. 74 (1993) R1.
[2] S.D. Gunapala, S.V. Bandara, Quantum Well Infrared Photodetector (QWIP) Focal Plane Arrays, Semiconductors and Semimetals, 62, Academic Press, 1999, pp. 197–282.
[3] S.D. Gunapala, S.V. Bandara, J.K. Liu, S.B. Rafol, J.M. Mumolo, IEEE Trans. Elec. Dev. 50 (2003) 2353.
[4] S.V. Bandara, S.D. Gunapala, F.M. Reininger, J.K. Liu, S.B. Rafol, J.M. Mumolo, D.Z. Ting, R.W. Chuang, T.Q. Trinh, J.M. Fastenau, A.W.K. Liu, SPIE 5074 (2003) 787.
[5] W. Cabanski, R. Breiter, R. Koch, K.H. Mauk, W. Rode, J. Ziegler, K. Eberhardt, R. Oelmaier, H. Schneider, M. Walther, Proc. SPIE 4028 (2000) 113.
[6] K.K. Choi, S.V. Bandara, S.D. Gunapala, W.K. Liu, J.M. Fastenau, J. Appl. Phys. 91 (2002) 5230.
[7] S.V. Bandara, S.D. Gunapala, J.K. Liu, E.M. Luong, J.M. Mumolo, W. Hong, D.K. Sengupta, M.J. McKelvey, Appl. Phys. Lett. 72 (1998) 2427.
[8] S.V. Bandara, S.D. Gunapala, J.K. Liu, S.B. Rafol, J.M. Mumolo, D.Z. Ting, Array of QWIPs With Spatial Separation of Multiple Colors, NASA Tech. Briefs, vol. 26(5), 8a, 2002.
[9] S.V. Bandara, S.D. Gunapala, J.K. Liu, S.B. Rafol, D.Z. Ting, J.M. Mumolo, R.W. Chuang, T.Q. Trinh, J.H. Liu, K.K. Choi, M. Jhabvala, J.M. Fastenau, A.W.K. Liu, Infrared Phys. & Tech. 44 (2003) 369.
[10] F.M. Reininger, Infrared Phys. & Tech. 42 (2001) 345.
[11] M. Jhabvala, S.D. Gunapala, D. Reuter, K.K. Choi, S.V. Bandara, J. Liu, A. La, S. Banks, J. Cho, T. Hwang, S. Tsay, D. Rafol, H. Huet, N. Chauvet, T. Huss, Infrared Phys. & Tech. 44 (2003) 445.
[12] J.Y. Andersson, L. Lundqvist, Z.F. Paska, J. Appl. Phys. 71 (1991) 3600.
[13] H.C. Liu, J. Li, J.R. Thompson, Z.R. Wasilewski, M. Buchanan, J.G. Simmons, IEEE Elec. Dev. Lett. 14 (1993) 566.
[14] L.C. Lenchyshyn, H.C. Liu, M. Buchanan, Z.R. Wasilewski, J. Appl. Phys. 79 (1996) 8091.